

## Article

# Enhanced Energy Storage Properties of La-Doped $\text{Sr}_{0.6}\text{Ba}_{0.4}\text{Nb}_2\text{O}_6$ Relaxor Ferroelectric Ceramics Prepared by Spark Plasma Sintering

Yingying Zhao <sup>1,\*</sup> , Xiao Liu <sup>1</sup>, Xiaoyu Zhang <sup>2</sup> and Huiling Du <sup>1,\*</sup> 

<sup>1</sup> College of Materials Science and Engineering, Xi'an University of Science and Technology, Xi'an 710054, China; liuxiao@xust.edu.cn

<sup>2</sup> State Key Laboratory for Mechanical Behavior of Materials, School of Materials Science and Engineering, Xi'an Jiaotong University, Xi'an 710049, China; xyzhang918@163.com

\* Correspondence: yyzhao@xust.edu.cn (Y.Z.); hldu@xust.edu.cn (H.D.)

**Abstract:** In this work, La-doped  $\text{Sr}_{0.6}\text{Ba}_{0.4}\text{Nb}_2\text{O}_6$  ferroelectric ceramics were fabricated by the conventional solid state reaction method (CS) and spark plasma sintering (SPS), respectively. The microstructure, phase structure, dielectric properties, relaxor behavior, ferroelectric and energy storage properties were investigated and compared to indicate the effects of spark plasma sintering on their performances. The results show that the grain shape changes from columnar to isometric crystal and the grain size decreases obviously after spark plasma sintering. The dielectric constant of the CS sample and the SPS sample both show a typical relaxor behavior with obvious frequency dispersion. The diffusion parameters ( $\gamma$ ) of both CS sample and SPS sample are close to 2 and all the samples present slim polarization–electric (P-E) loops, which verify the relaxor behavior. Moreover, the breakdown strength,  $E_b$ , and discharge energy storage density,  $W_{\text{rec}}$ , of La-doped  $\text{Sr}_{0.6}\text{Ba}_{0.4}\text{Nb}_2\text{O}_6$  ferroelectric ceramics prepared by SPS are improved significantly. This work provides guidance for improving the energy storage performance of ferroelectric ceramics with tungsten bronze structures by decreasing the grain size through adopting a different sintering method.

**Keywords:** spark plasma sintering; strontium barium niobate; energy storage performance; relaxor ferroelectric ceramics



**Citation:** Zhao, Y.; Liu, X.; Zhang, X.; Du, H. Enhanced Energy Storage Properties of La-Doped  $\text{Sr}_{0.6}\text{Ba}_{0.4}\text{Nb}_2\text{O}_6$  Relaxor Ferroelectric Ceramics Prepared by Spark Plasma Sintering. *Materials* **2022**, *15*, 4360. <https://doi.org/10.3390/ma15124360>

Academic Editor: Miguel Alguero

Received: 19 May 2022

Accepted: 17 June 2022

Published: 20 June 2022

**Publisher's Note:** MDPI stays neutral with regard to jurisdictional claims in published maps and institutional affiliations.



**Copyright:** © 2022 by the authors. Licensee MDPI, Basel, Switzerland. This article is an open access article distributed under the terms and conditions of the Creative Commons Attribution (CC BY) license (<https://creativecommons.org/licenses/by/4.0/>).

## 1. Introduction

With the environmental problem caused by the consumption of fossil energy, renewable energy and energy storage technology need to be developed urgently. Due to the ultrafast charge and discharge rate, high power density and good cycling performance of dielectric capacitors, they have great potential in energy storage devices, including smart power grids, impulse power, electric vehicles and so on [1–4]. There are four main categories of dielectric energy materials, including linear dielectrics, ferroelectrics (FE), relaxor ferroelectrics (RFE) and antiferroelectrics (AFE). Among them, ferroelectric and antiferroelectric ceramics exhibit great potential in energy-storage fields due to small residue polarization  $P_r$  [5–7]. However, most antiferroelectrics with excellent properties contain lead, which would cause serious environment problems. Other AFE systems like  $\text{AgNbO}_3$ -based materials show inferior anti-fatigue performance. Consequently, RFE ceramics have unique advantages when applied in energy storage devices because they have a slim P-E loop.

Strontium barium niobate, SBN ( $\text{Sr}_x\text{Ba}_{1-x}\text{Nb}_2\text{O}_6$ ,  $0.25 \leq x \leq 0.75$ ), as a lead-free relaxor ferroelectric material, is a promising lead-free alternative. SBN has an unfilled tetragonal tungsten bronze structure with a formula of  $(\text{A}1)_2(\text{A}2)_4\text{C}_4(\text{B}1)_2(\text{B}2)_8\text{O}_{30}$ . The B1 and B2 sites are occupied by Nb ions, which form  $\text{NbO}_6$  octahedra, combining O ions [8,9]. Sr ions occupy both the A1 site and the larger A2 site, whereas the larger Ba ions occupy the

A2 site only. The smaller C site remains empty [10,11]. Moreover, SBN ceramics transition from normal ferroelectrics to relaxor ferroelectrics when the Sr/Ba increases [10]. It is well known that  $E_b$  has a greater influence on the energy storage density compared to the permittivity [12], and the  $E_b$  is closely related to grain size. Consequently, there are many studies about refining the grain size of ferroelectrics by introducing different elements and changing the sintering method [13–15]. Song et al. introduced a glass addition and prepared the SBN ceramics by conventional solid state reaction method, which obtained a decreased grain size and improved breakdown strength [16]. Xiu et al. prepared SBN glass-ceramics and refined the grain size by introducing a glass addition [17]. Moreover, it has been reported that the grain size can also be refined by changing the sintering method. Zhao et al. prepared  $\text{Bi}_{0.5}\text{Na}_{0.5}\text{TiO}_3$  (BNT)-based ceramics and multilayer ceramic capacitors by a two-step sintering method and obtained obviously decreased grain size [18]. Huang et al. prepared  $\text{Ba}_{0.4}\text{Sr}_{0.6}\text{TiO}_3@ \text{SiO}_2$  dense ceramics via the spark plasma sintering method and obtained sub-micron grain size [19]. Spark plasma sintering (SPS) technology has been employed in many systems, including  $\text{Ba}_{0.4}\text{Sr}_{0.6}\text{TiO}_3$ ,  $\text{Pb}(\text{Zr},\text{Ti})\text{O}_3$  and so on. During SPS process, direct current, high mechanical pressure and low voltage are applied, resulting in the ultrahigh heating and cooling rates and a very short sintering time. Thus, the microstructures and grains growth of ceramics prepared by SPS can be controlled well [19–22].

While due to the grains of SBN ceramics often are anisometric and columnar, the microstructure of SBN ceramics prepared by CS is not very dense, as a result of which the breakdown strength and the energy storage performance are poor. Therefore, in this work, the La-doped  $\text{Sr}_{0.6}\text{Ba}_{0.4}\text{Nb}_2\text{O}_6$  ferroelectric ceramics were prepared by CS and SPS, respectively. The doping of  $\text{La}^{3+}$  can reduce the ferroelectric domain size further and enhance the relaxor behavior. The morphology, dielectric response, relaxor behavior and energy storage properties are compared. With the SPS sintering method, the grain size decreases obviously, and the grain shape changes from a columnar to an isometric crystal. Consequently, increased breakdown strength and higher energy storage efficiency have been obtained.

## 2. Experimental Procedures

The conventional solid state reaction method (CS) and spark plasma sintering (SPS) technology were used to prepare  $\text{Sr}_{0.585}\text{Ba}_{0.4}\text{La}_{0.02}\text{Nb}_2\text{O}_6$  (SBN60-2La) ceramics. The raw materials were  $\text{BaCO}_3$  (99.9%),  $\text{SrCO}_3$  (99.9%),  $\text{La}_2\text{O}_3$  (99.9%) and  $\text{Nb}_2\text{O}_5$  (99.9%), which were all bought from the Alfa Aesar company. The samples are denoted as CS sample and SPS sample, respectively. The CS process was reported in a previous article [10] and the SBN60-2La samples in this work were sintered at 1350 °C for 4 h. For the SPS sample, the SBN60-2La powders were presintered by CS and then put into a graphite die with a diameter of 10 mm. In order to avoid contact between the powder and the die, a graphite foil was used in the SPS sintering process. Then the powders were sintered by SPS at 1000 °C for 5 min. Finally, the samples sintered by SPS were annealed at 900 °C for 2 h to remove the residual carbon caused by the graphite foil and die in SPS sintering process.

The phase structure of all the samples were detected by X-ray diffraction (XRD, X'Pert diffractometer with  $\text{Cu K}\alpha \lambda=0.15406$  nm) at room temperature. A scanning electron microscope (SEM, Hitachi S-2700) was used to detect the surface microstructure and fracture microstructure. In order to detect the surface microstructure, the SBN60-2La ceramics prepared by SPS were thermal etched at 1000 °C for 20 min and the SBN60-2La ceramics prepared by CS were thermal etched at 1250 °C for 10 min. The HIOKI LCR Hitester was used to measure the dependence of the dielectric response within the temperature range of  $-50$  °C– $200$  °C. The Precision Premier II (from Radiant Company) with a high voltage amplifier was used to characterize the P-E loops.

### 3. Results and Discussions

Figure 1 depicts the comparison between SEM images of SBN60-2La ceramics prepared by CS and SPS. The surface morphologies and the fracture surface morphologies of the CS sample and SPS sample are shown in Figure 1a–d, respectively. Obviously, it can be seen from Figure 1a,b that the CS samples show anisometric and columnar shaped grains, while the grains of SPS samples are isometric and the size of the SPS samples is much smaller than that of the CS samples. The average grain size of the SPS sample is 1.22  $\mu\text{m}$ , while the CS sample has an average grain size of 6.12  $\mu\text{m}$ . Moreover, in order to investigate the detailed microstructure, the fracture surface morphologies of the CS sample and SPS sample are shown in Figure 1c,d, respectively. It can be seen that the microstructure of SBN60-2La, prepared by SPS, is denser. Due to the columnar shape grain of CS sample, the microstructure is not dense enough and obvious pores between the grains can be seen in Figure 1c, while the SPS sample in Figure 1d shows a much more compact microstructure with a few very small pores. This is attributed to the fast sintering rate and short sintering time of the SPS sintering method.

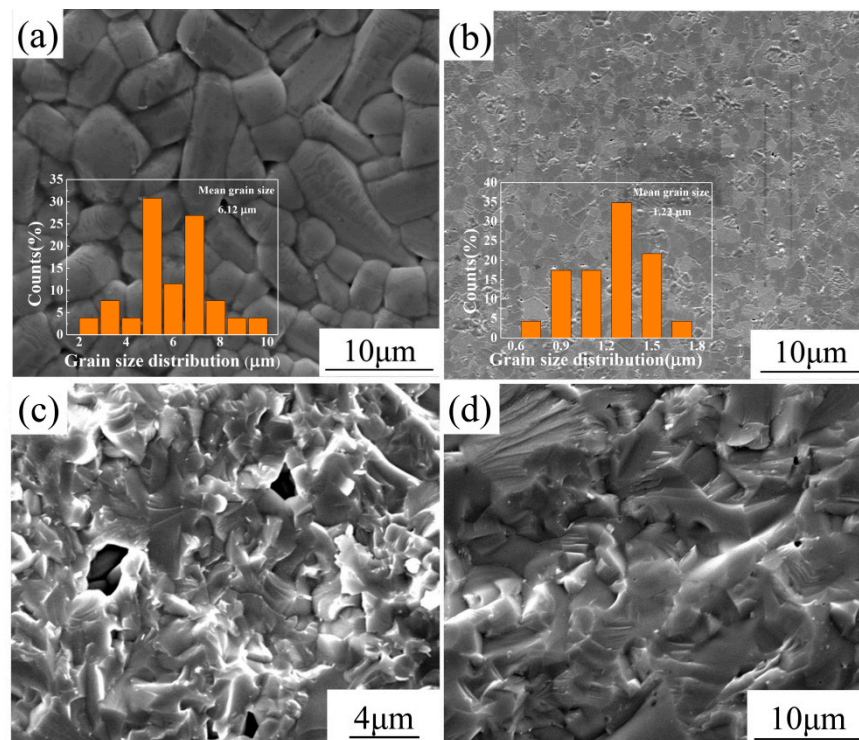
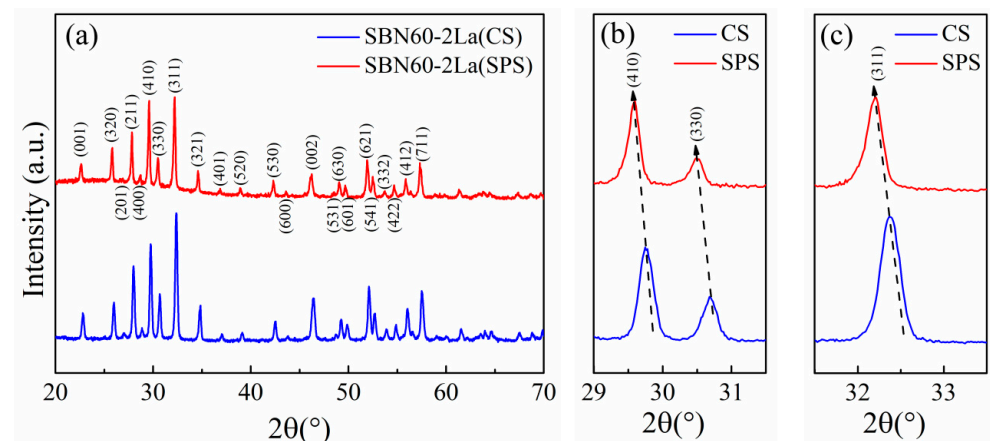


**Figure 1.** The surface morphologies and the fracture surface morphologies of SBN60-2La ceramics prepared by CS and SPS: (a) CS, (b) SPS, (c) CS, (d) SPS.

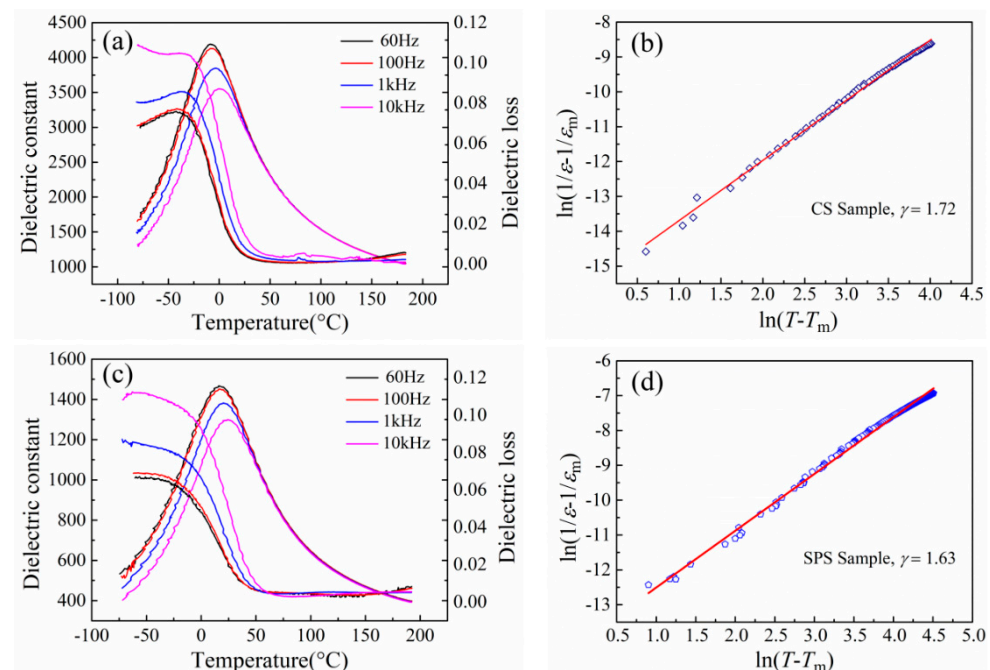
The XRD patterns of the CS sample and SPS sample are illustrated in Figure 2. It can be seen from Figure 2a that both the CS sample and SPS sample show a pure tetragonal tungsten bronze structure without an impurity phase, which indicates that the SBN60-2La ceramics prepared by SPS has good crystallinity. The (410), (330) and (311) peak profiles are presented in Figure 2b,c. It can be seen that the peak of SPS sample shows slight shifts towards lower  $2\theta$  values, indicating a gradual increase in lattice parameters and unit cell volume. This maybe because the carbon element caused by the graphite foil and die used in SPS sintering may enter into the SBN60-2La sample.

Figure 3 depicts the temperature dependence of dielectric properties and the relaxor properties of SBN60-2La ceramics prepared by CS and SPS. It can be seen from Figure 3a,c that when the temperature is below the temperature ( $T_m$ ) of the maximum dielectric constant, both the CS sample and SPS sample show a distinct frequency-dependent behavior. With the frequency increasing, the  $T_m$  shifts towards higher temperature. Both

the CS sample and SPS sample show typical relaxor behavior with obvious frequency dispersion. Moreover, it can be seen that the dielectric constant of SPS samples is much smaller than that of CS samples. This phenomenon is closely related with the grain size. The grain size effects on the dielectric properties of perovskite ferroelectric ceramics have been widely reported. The ceramics with smaller grain size show a lower dielectric constant value and the samples with uniform grain size distribution show a higher dielectric constant value when the grain size is almost same [23–25]. So, it can be concluded that the smaller dielectric constant value of SPS samples is attributed to the smaller grain size of SPS sample. Moreover, the dielectric loss of both the CS sample and SPS sample shows a high value below the  $T_m$ , and the dielectric loss decreases rapidly to a very small value when the temperature increases.



**Figure 2.** (a) X-ray diffraction patterns at room temperature, (b) (410) and (330) peak profiles, (c) (311) peak profiles for the CS sample and SPS sample.



**Figure 3.** The dielectric properties of SBN60-2La ceramics: the temperature dependence of dielectric properties of (a) CS sample; (b) SPS sample, plots of  $\ln(1/\epsilon - 1/\epsilon_m)$  versus  $\ln(T - T_m)$  at 1 kHz; (c) CS sample; (d) SPS sample.

In order to investigate the diffuseness degree of the CS sample and SPS sample, the modified Curie–Weiss law as follows was used to fit:

$$(1/\varepsilon - 1/\varepsilon_m) = (T - T_m)^\gamma / C \quad (1)$$

where  $\varepsilon_m$  represents the maximum value of the dielectric permittivity at  $T_m$ , the  $\gamma$  ( $1 \leq \gamma \leq 2$ ) value indicates the diffuseness and  $C$  is the Curie constant. Normally,  $\gamma = 1$  suggests normal ferroelectric with a Curie–Weiss behavior, while  $\gamma = 2$  represents for an ideal relaxor ferroelectric. In order to investigate the influence of the SPS sintering method on the relaxor behavior of the SBN60-2La ceramics, the plots of  $\ln(1/\varepsilon - 1/\varepsilon_m)$  as a function of  $\ln(T - T_m)$  at 1 kHz of CS sample and SPS sample are shown in Figure 3b,d, respectively. The diffuseness value  $\gamma$  of CS sample and SPS sample are 1.63 and 1.72, respectively, which are both close to 2. This indicates that both the CS sample and SPS sample show a typical diffuse transition. The  $\gamma$  value of SPS sample is close to that of the CS sample, which indicates that the SPS sintering method has little influence on the relaxor behavior of the SBN60-2La ceramics.

The P-E loops of SBN60-2La ceramics prepared by CS and SPS are exhibited in Figure 3a,b, respectively. It can be observed that La-doped SBN ferroelectric ceramics show a very slim P-E loop, which verifies the relaxor feature. This is consistent with the results obtained in the dielectric measurement. Based on the P-E loops given in Figure 3a,b, the total energy storage density ( $W_{\text{total}}$ ), the recoverable energy storage density ( $W_{\text{rec}}$ ) and the energy storage efficiency ( $\eta$ ) could be calculated by using the following formula (2 and 5):

$$W_{\text{total}} = \int_0^{P_{\text{max}}} E dP \quad (2)$$

$$W_{\text{rec}} = \int_{P_r}^{P_{\text{max}}} E dP \quad (3)$$

$$\eta = W_{\text{rec}} / W_{\text{total}}. \quad (4)$$

As plotted in Figure 3a,b, the breakdown electric field of the SPS sample is much higher than the CS sample. Because the sample thickness in this work is thick (1 mm), the measurable electric field and the obtained breakdown strength is relatively low. For the CS sample, the polarization shows a rapid increase under a low electric field, limiting the enhancement of the energy storage performance to a great extent. Under the same electric field, the maximum polarization value ( $P_{\text{max}}$ ) of the SPS sample is a little smaller than that of CS sample. The P-E loop of SPS sample is more slant than that of the CS sample, which indicates the delayed polarization saturation. When the applied electric field increases, the maximum polarization can achieve a higher value, which can enhance the energy storage properties [26]. The calculated  $W_{\text{total}}$ ,  $W_{\text{rec}}$  and  $\eta$  of the CS sample and SPS sample are shown in Figure 4c,d. It can be seen that the  $W_{\text{total}}$  and  $W_{\text{rec}}$  of the SPS sample are much higher than that of the CS sample, which can be attributed to the higher breakdown strength of the SPS sample. It is well known that the breakdown strength  $E_b$  is closely related with the grain size (Ga):  $E_b \propto (\text{Ga})^{-a}$ , where the exponent value is 0.2~0.4 [27]. The  $E_b$  is inversely proportional to the grain size. Dense microstructure and small grain size are beneficial to the enhancement of  $E_b$ . Hence, the decreased grain size and the denser microstructure of SBN60-2La prepared by SPS in this work make an important contribution to the improvement of  $E_b$ . The energy storage efficiency,  $\eta$ , of the CS sample is a little higher than that of the SPS sample, which is the result of the fast polarization saturation. However, both the SBN60-2La ceramics prepared by CS and SPS obtain a high efficiency  $\eta$  value, which is higher than 85%. This can be attributed to the slim P-E loop caused by the relaxor feature of the La modifier. The electric parameters of the SBN60-2La ceramics prepared by CS and SPS are summarized in Table 1.

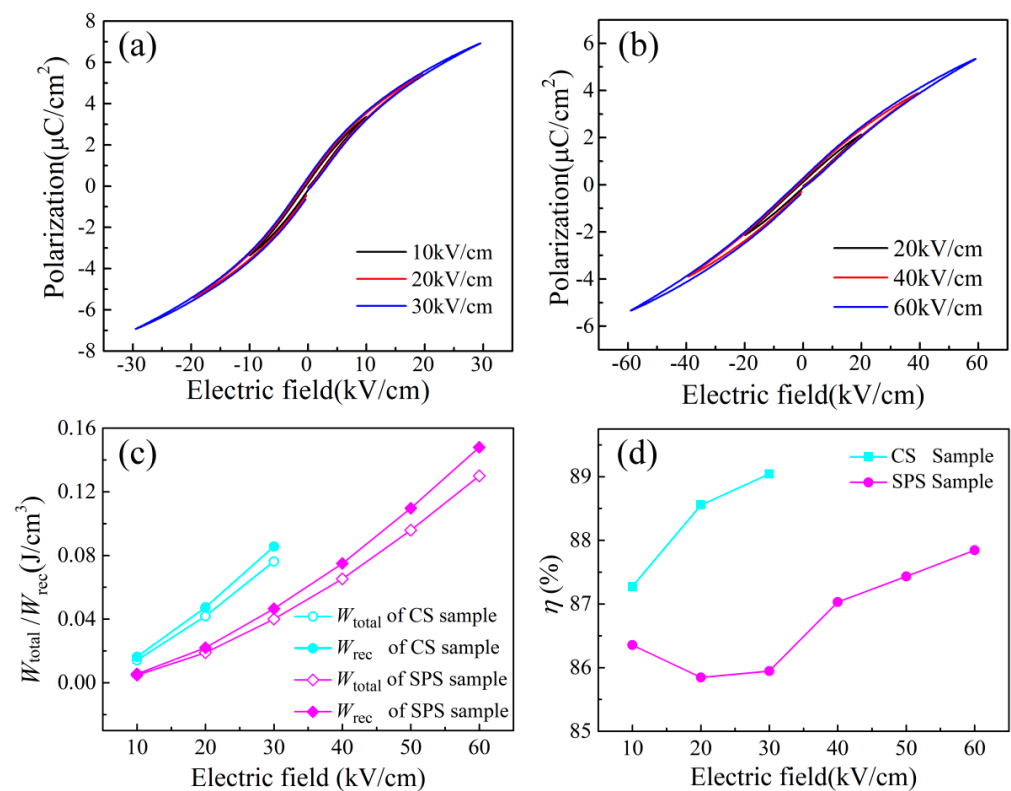


**Figure 4.** P-E loops measures with different electric fields of SBN60–2La prepared by (a) CS and (b) SPS; (c)  $W_{total}$ ,  $W_{rec}$  and (d)  $\eta$  of the CS sample and SPS sample.

**Table 1.** The electric parameters of SBN60-2La prepared by CS and SPS.

Ceramics	Relative Density	Mean Grain Size ( $\mu\text{m}$ )	$T_m/1$ kHz ( $^{\circ}\text{C}$ )	$\gamma/1$ kHz	$W_{total}$ ( $\text{J}\cdot\text{cm}^{-3}$ )	$W_{rec}$ ( $\text{J}\cdot\text{cm}^{-3}$ )	$\eta$
CS Sample	95.3%	6.12	−3	1.72	0.086	0.076	89.0%
SPS Sample	98.5%	1.22	20	1.63	0.130	0.148	87.8%

#### 4. Conclusions

La-doped  $\text{Sr}_{0.6}\text{Ba}_{0.4}\text{Nb}_2\text{O}_6$  ferroelectric ceramics were prepared by the conventional solid state reaction method (CS) and spark plasma sintering (SPS), respectively. The grain shape changes from a columnar to an isometric crystal and the grain size decreases obviously after spark plasma sintering. Both the CS sample and SPS sample show obvious frequency dispersion and a diffuseness value  $\gamma$  close to 2, which indicates their classical relaxor behavior. All the samples show slim P-E loops, which verify the relaxor behavior. Moreover, the SPS sample has a higher  $E_b$  and  $W_{rec}$  due to the smaller grain size and denser microstructure. All the samples show a high  $\eta$  value of over 85%. This work provides guidance for improving the energy storage properties through refining grain size by SPS for strontium barium niobate ferroelectric ceramics.

**Author Contributions:** Conceptualization, Y.Z. and H.D.; Experiment, Y.Z. and X.Z.; Investigation, Y.Z., X.Z. and X.L.; writing—original draft, Y.Z.; writing—review and editing, X.L. and H.D. All authors have read and agreed to the published version of the manuscript.

**Funding:** This research was funded by the National Natural Science Foundation of China (52172099), Natural Science Basic Research Plan in Shaanxi Province of China (2021JQ-566), Provincial Joint Fund of Shaanxi (2021JLM-28), Scientific Research Plan Projects of Shaanxi Province Education Department (21JK0756) and Science and Technology Plan Project of Xi'an Beilin District of Shaanxi Province (GX2113).

**Institutional Review Board Statement:** Not applicable.

**Informed Consent Statement:** Not applicable.

**Data Availability Statement:** Not applicable.

**Conflicts of Interest:** The authors declare no conflict of interest.

## References

1. He, J.; Liu, X.; Zhao, Y.; Du, H.; Zhang, T.; Shi, J. Dielectric Stability and Energy-Storage Performance of BNT-Based Relaxor Ferroelectrics through Nb<sup>5+</sup> and Its Excess Modification. *ACS Appl. Electron. Mater.* **2022**, *4*, 735–743. [[CrossRef](#)]
2. Kang, R.; Wang, Z.; Lou, X.; Liu, W.; Shi, P.; Zhu, X.; Guo, X.; Li, S.; Sun, H.; Zhang, L.; et al. Energy storage performance of Bi<sub>0.5</sub>Na<sub>0.5</sub>TiO<sub>3</sub>-based relaxor ferroelectric ceramics with superior temperature stability under low electric fields. *Chem. Eng. J.* **2021**, *410*, 128376. [[CrossRef](#)]
3. Zhou, W.; Li, T.; Yuan, M.; Li, B.; Zhong, S.; Li, Z.; Liu, X.; Zhou, J.; Wang, Y.; Cai, H.; et al. Decoupling of inter-particle polarization and intra-particle polarization in core-shell structured nanocomposites towards improved dielectric performance. *Energy Storage Mater.* **2021**, *42*, 1–11. [[CrossRef](#)]
4. Shi, J.; Liu, X.; Zhu, F.; Tian, W.; Xia, Y.; Li, T.; Rao, R.; Zhang, T.; Liu, L. Oxygen vacancy migration and its lattice structural origin in A-site non-stoichiometric bismuth sodium titanate perovskites. *J. Mater.* **2022**, *8*, 719–729. [[CrossRef](#)]
5. Wang, G.; Lu, Z.; Li, Y.; Li, L.; Ji, H.; Feteira, A.; Zhou, D.; Wang, D.; Zhang, S.; Reaney, I.M. Electroceramics for High-Energy Density Capacitors: Current Status and Future Perspectives. *Chem. Rev.* **2021**, *121*, 6124–6172. [[CrossRef](#)]
6. Li, D.; Zeng, X.; Li, Z.; Shen, Z.Y.; Hao, H.; Luo, W.; Wang, X.; Song, F.; Wang, Z.; Li, Y. Progress and perspectives in dielectric energy storage ceramics. *J. Adv. Ceram.* **2021**, *10*, 675–703. [[CrossRef](#)]
7. Yang, Z.; Du, H.; Jin, L.; Poelman, D. High-performance lead-free bulk ceramics for electrical energy storage applications: Design strategies and challenges. *J. Mater. Chem. A* **2021**, *9*, 18026–18085. [[CrossRef](#)]
8. Bhaumik, I.; Ganesamoorthy, S.; Bhatt, R.; Subramanian, N.; Karnal, A.K.; Gupta, P.K.; Takekawa, S.; Kitamura, K. Influence of cerium doping on the dielectric relaxation of Sr<sub>0.75</sub>Ba<sub>0.25</sub>Nb<sub>2</sub>O<sub>6</sub> single crystal grown by the double crucible Stepanov technique. *J. Alloys Compd.* **2015**, *621*, 26–29. [[CrossRef](#)]
9. Said, M.; Velayutham, T.S.; Gan, W.C.; Abd Majid, W.H. The structural and electrical properties of Sr<sub>x</sub>Ba<sub>(1-x)</sub>Nb<sub>2</sub>O<sub>6</sub> (SBN) ceramic with varied composition. *Ceram. Int.* **2015**, *41*, 7119–7124. [[CrossRef](#)]
10. Zhao, Y.; Wang, J.; Zhang, L.; Shi, X.; Liu, S.; Zhang, D. Relaxor transition and properties of Mn-doped Sr<sub>x</sub>Ba<sub>1-x</sub>Nb<sub>2</sub>O<sub>6</sub> ferroelectric ceramics. *Ceram. Int.* **2016**, *42*, 16697–16702. [[CrossRef](#)]
11. Zhao, Y.; Wang, J.; Zhang, L.; Liu, S.; Zhang, D.; Wang, X. Large activation energy in aged Mn-doped Sr<sub>0.4</sub>Ba<sub>0.6</sub>Nb<sub>2</sub>O<sub>6</sub> ferroelectric ceramics. *RSC Adv.* **2017**, *7*, 26894–26902. [[CrossRef](#)]
12. Wang, Z.; Zhang, L.; Kang, R.; Yang, W.; He, L.; Mao, P.; Lou, X.; Zhang, L.; Wang, J. (Bi<sub>0.5</sub>Na<sub>0.5</sub>)TiO<sub>3</sub>-based relaxor ferroelectrics with enhanced energy-storage density and efficiency under low/moderate-fields via average ionic polarizability design. *Chem. Eng. J.* **2022**, *431*, 133716. [[CrossRef](#)]
13. Ma, W.; Fan, P.; Salamon, D.; Kongparakul, S.; Samart, C.; Zhang, T.; Zhang, G.; Jiang, S.; Chang, J.J.; Zhang, H. Fine-grained BNT-based lead-free composite ceramics with high energy-storage density. *Ceram. Int.* **2019**, *45*, 19895–19901. [[CrossRef](#)]
14. Luo, C.; Wei, Y.; Feng, Q.; Wang, M.; Luo, N.; Yuan, C.; Zhou, C.; Fujita, T.; Xu, J. Significantly enhanced energy-storage properties of Bi<sub>0.47</sub>Na<sub>0.47</sub>Ba<sub>0.06</sub>TiO<sub>3</sub>-CaHfO<sub>3</sub> ceramics by introducing Sr<sub>0.7</sub>Bi<sub>0.2</sub>TiO<sub>3</sub> for pulse capacitor application. *Chem. Eng. J.* **2022**, *429*, 132165. [[CrossRef](#)]
15. Shi, P.; Zhu, X.; Lou, X.; Yang, B.; Liu, Q.; Kong, C.; Yang, S.; He, L.; Kang, R.; Zhao, J. Tailoring ferroelectric polarization and relaxation of BNT-based lead-free relaxors for superior energy storage properties. *Chem. Eng. J.* **2022**, *428*, 132612. [[CrossRef](#)]
16. Song, J.; Han, L.; Liu, T.; Feng, Q.; Luo, Z.; Lu, A. Microstructures and energy storage properties of BSN ceramics with crystallizable glass addition. *J. Mater. Sci.-Mater. Electron.* **2018**, *29*, 5934–5943. [[CrossRef](#)]
17. Xiu, S.; Xiao, S.; Xue, S.; Shen, B.; Zhai, J. Crystallization kinetics behaviour and dielectric properties of strontium barium niobate-based glass-ceramics. *J. Mater. Sci.-Mater. Electron.* **2016**, *27*, 5324–5330. [[CrossRef](#)]
18. Zhao, P.; Chen, L.; Li, L.; Wang, X. Ultrahigh energy density with excellent thermal stability in lead-free multilayer ceramic capacitors via composite strategy design. *J. Mater. Chem. A* **2021**, *9*, 25914–25921. [[CrossRef](#)]
19. Huang, Y.H.; Wu, Y.J.; Liu, B.; Yang, T.N.; Wang, J.J.; Li, J.; Chen, L.Q.; Chen, X.M. From core-shell Ba<sub>0.4</sub>Sr<sub>0.6</sub>TiO<sub>3</sub>@SiO<sub>2</sub> particles to dense ceramics with high energy storage performance by spark plasma sintering. *J. Mater. Chem. A* **2018**, *6*, 4477–4484. [[CrossRef](#)]
20. Zhai, Y.; Xie, X.; Zhou, R.; Li, X.; Liu, X.; Liu, S. High performance room temperature ferroelectric barium strontium titanate ceramics by spark-plasma-sintering ultrafine nanocrystals. *Ceram. Int.* **2019**, *45*, 15526–15531. [[CrossRef](#)]
21. Ochoa, D.A.; Suñol, F.; Rubio-Marcos, F.; García, J.E. Enhancement of piezoelectric properties stability of submicron-structured piezoceramics obtained by spark plasma sintering. *J. Eur. Ceram. Soc.* **2018**, *38*, 4659–4663. [[CrossRef](#)]
22. Tokita, M. Progress of Spark Plasma Sintering (SPS) Method, Systems, Ceramics Applications and Industrialization. *Ceramics* **2021**, *4*, 160–198. [[CrossRef](#)]
23. Luan, W.L.; Gao, L.; Guo, J.K. Size effect on dielectric properties of fine-grained BaTiO<sub>3</sub> ceramics. *Ceram. Int.* **1999**, *25*, 727–729. [[CrossRef](#)]
24. Hanani, Z.; Mezzane, D.; Amjoud, M.; Fourcade, S.; Razumnaya, A.G.; Luk'yanchuk, I.A.; Goune, M. Enhancement of dielectric properties of lead-free BCZT ferroelectric ceramics by grain size engineering. *Superlattices Microst.* **2019**, *127*, 109–117. [[CrossRef](#)]

25. Tan, Y.Q.; Zhang, J.L.; Wu, Y.Q.; Wang, C.L.; Koval, V.; Shi, B.G.; Ye, H.T.; McKinnon, R.; Viola, G.; Yan, H.X. Unfolding grain size effects in barium titanate ferroelectric ceramics. *Sci. Rep.* **2015**, *5*, 9953. [[CrossRef](#)]
26. Shi, J.; Zhao, Y.; He, J.; Li, T.; Zhu, F.; Tian, W.; Liu, X. Deferred Polarization Saturation Boosting Superior Energy-Storage Efficiency and Density Simultaneously under Moderate Electric Field in Relaxor Ferroelectrics. *ACS Appl. Energ. Mater.* **2022**, *5*, 3436–3446. [[CrossRef](#)]
27. Yang, L.; Kong, X.; Li, F.; Hao, H.; Cheng, Z.; Liu, H.; Li, J.F.; Zhang, S. Perovskite lead-free dielectrics for energy storage applications. *Prog. Mater. Sci.* **2019**, *102*, 72–108. [[CrossRef](#)]